nature astronomy

LETTERS

https://doi.org/10.1038/s41550-021-01306-2

Check for updates

Dynamical evidence for Phobos and Deimos as remnants of a disrupted common progenitor

Amirhossein Bagheri[1]✉, Amir Khan[1,2], Michael Efroimsky[3], Mikhail Kruglyakov[1] and Domenico Giardini[1]

The origin of the Martian moons, Phobos and Deimos, remains elusive. While the morphology and their cratered surfaces suggest an asteroidal origin[1–3], capture has been questioned because of potential dynamical difficulties in achieving the current near-circular, near-equatorial orbits[4,5]. To circumvent this, in situ formation models have been proposed as alternatives[6–9]. Yet, explaining the present location of the moons on opposite sides of the synchronous radius, their small sizes and apparent compositional differences with Mars[2] has proved challenging. Here, we combine geophysical and tidal-evolution modelling of a Mars–satellite system to propose that Phobos and Deimos originated from disintegration of a common progenitor that was possibly formed in situ. We show that tidal dissipation within a Mars–satellite system, enhanced by the physical libration of the satellite, circularizes the post-disrupted eccentric orbits in <2.7 Gyr and makes Phobos descend to its present orbit from its point of origin close to or above the synchronous orbit. Our estimate for Phobos's maximal tidal lifetime is considerably less than the age of Mars, indicating that it is unlikely to have originated alongside Mars. Deimos initially moved inwards, but never transcended the co-rotation radius because of insufficient eccentricity and therefore insufficient tidal dissipation. Whereas Deimos is very slowly receding from Mars, Phobos will continue to spiral towards and either impact with Mars or become tidally disrupted on reaching the Roche limit in $\lesssim$39 Myr.

Tidal interactions between celestial bodies result in energy dissipation and drive systems towards equilibrium states, in part by pushing eccentricity and obliquity to zero and spin rates towards synchronization. This evolution is governed by the dissipative properties (including the frequency-scaling laws) of both the planet and the moons[10]. To determine the orbital history of a Mars–satellite system, we use up-to-date geophysical data for Mars and its satellites, including Martian seismic data from the currently operating InSight mission[11,12], laboratory-based viscoelastic models[13] describing Mars's rheology[14], and a comprehensive tidal-evolution model based on the extended Darwin–Kaula theory of tides[15], including the contribution from a satellite's physical libration in longitude. We consider Mars–Phobos and Mars–Deimos as separate orbital systems and integrate the semi-major axis (a), eccentricity (e), Mars's spin rate ($\dot{\theta}$) and inclinations of the satellites (i) backwards in time (t), starting from the current configuration. Our tidal model includes degree-2 and -3 inputs, because of the proximity of the moons to Mars. Although Phobos and Deimos are tidally locked, their uniform rotational motion is modified by physical libration arising from the time-varying gravitational torque exerted by Mars on their dynamical figures, which enhances tidal dissipation[16]. This effect is more pronounced for Phobos than Deimos, owing to Phobos's higher eccentricity and triaxiality. All properties are summarized in Supplementary Table 1.

For a non-librating planet hosting a satellite librating about a 1:1 spin–orbit resonance, the tidal rates of the semi-major axis and eccentricity can be written in terms of the mean motion (n), satellite libration amplitude ($\mathcal{A}$), and planet and satellite quality functions ($K_l = k_l/Q_l$ and $K'_l = k'_l/Q'_l$), masses (M and M'), spin rates ($\dot{\theta}$ and $\dot{\theta}'$) and radii (R and R'):

$$\frac{\mathrm{d}a}{\mathrm{d}t} = \frac{G(M+M')M'}{na^2\quad M}\left(\frac{R}{a}\right)^5\left[\mathcal{F}(K_l,\dot{\theta},n,e) + \mathcal{F}(K'_l,\dot{\theta}',n,e) + \mathcal{G}(K'_l,n,e,\mathcal{A})\right], \tag{1}$$

$$\frac{\mathrm{d}e}{\mathrm{d}t} = \frac{G(M+M')M'}{na^3\quad M}\left(\frac{R}{a}\right)^5\left[\mathcal{L}(K_l,\dot{\theta},n,e) + \mathcal{L}(K'_l,\dot{\theta}',n,e) + \mathcal{H}(K'_l,n,e,\mathcal{A})\right], \tag{2}$$

where G is the gravitational constant, unprimed and primed variables refer to those of the planet and the satellite, respectively, and the terms in the square brackets represent the dissipation due to the main tides on the planet ($\mathcal{F}(K_l,\dot{\theta},n,e)$ and $\mathcal{L}(K_l,\dot{\theta},n,e)$), the main tides on the satellite ($\mathcal{F}(K'_l,\dot{\theta}',n,e)$ and $\mathcal{L}(K'_l,\dot{\theta}',n,e)$), and satellite libration ($\mathcal{G}(K'_l,n,e,\mathcal{A})$ and $\mathcal{H}(K'_l,n,e,\mathcal{A})$). Inclination ($i$) of a satellite orbit on Mars's equator is governed by

$$\frac{\mathrm{d}i}{\mathrm{d}t} = n\sin i\,\frac{M'}{M}\left(\frac{R}{a}\right)^5\left[\mathcal{I}(K_l,\dot{\theta},n,i,e)\right], \tag{3}$$

where the term in square brackets refers to the main tides on the planet. Detailed expressions for the functions $\mathcal{F}$, $\mathcal{G}$, $\mathcal{L}$, $\mathcal{H}$ and $\mathcal{I}$ are given in Methods. To ensure precision, the functions were expanded to order 18 in eccentricity. Equations (1)–(3) were integrated backwards in time using a Runge–Kutta explicit iterative solver. We also track the planetocentric distances (R_p) of the two satellites, given by $R_\mathrm{p} = a(1-e^2)/(1+e\cos f)$, where f is the true anomaly. R_p assumes values in the interval $a(1-e) \le R_\mathrm{p} \le a(1+e)$, so a satellite always resides between the two circles. We shall compare the minimal distance of Deimos with the maximal distance of Phobos, and shall be particularly interested in the case where minimal $R_\mathrm{p}^{\mathrm{Deimos}} \le$ maximal $R_\mathrm{p}^{\mathrm{Phobos}}$ (Supplementary Section 2), that is, where the orbits of the moons intersect.

[1]Institute of Geophysics, ETH Zürich, Zurich, Switzerland. [2]Physik-Institut, University of Zürich, Zurich, Switzerland. [3]US Naval Observatory, Washington DC, USA. ✉e-mail: amirhossein.bagheri@erdw.ethz.ch

During the orbital evolution, Phobos undergoes 2:1 and 3:1 spin–orbit resonances with Mars's figure at $a = 3.8R_{Mars}$ and $a = 2.9R_{Mars}$, respectively, where R_{Mars} is the mean radius of Mars, and a 1:1 resonance with the Sun at $a = 2.6R_{Mars}$ when its pericentre rate equals the Martian mean motion. Deimos is affected by a 2:1 mean motion resonance with Phobos. These resonances result in rapid eccentricity changes Δe (ref. [17]). For Phobos, $\Delta e_{2:1}^{Mars} = 0.032$, $\Delta e_{3:1}^{Mars} = 0.002$ and $\Delta e_{1:1}^{Sun} = 0.0085$, whereas for Deimos, $\Delta e_{2:1}^{Phobos} = 0.002$. Finally, in the course of our integrations, we assume that the system has not been affected by any other planetary material.

To compute the quality functions, models of Mars, Phobos and Deimos are required. For Mars, self-consistently computed interior-structure models are obtained by inversion of geophysical data[14] (Supplementary Sections 3 and 4 and Supplementary Fig. 1), which include the degree-2 tidal amplitude in the form of the Love number (k_2) and the phase response (Q_2), mean density and mean moment of inertia (Supplementary Table 1). One of the main parameters that controls the orbital history of Phobos is the frequency dependence of tidal dissipation (through the exponent α)[14]. Current observations of a few of the largest low-frequency marsquakes are compatible with an effective mantle Martian seismic Q of approximately 300 (refs. [11,12]). These, together with the observation of the Phobos-induced tidal Q around 95 ± 10, suggest an α value in the range of 0.25–0.35, in agreement with previous studies[14,18]. For our nominal cases, we employ $\alpha = 0.27$. Densities of Phobos and Deimos are $<2\,\mathrm{g\,cm^{-3}}$, implying porous and therefore highly dissipative, yet weakly bonded, aggregates[19,20]. This assumption is based on the moons' ability to sustain sharp features (such as ubiquitous grooves and fractures)[21], their ability to wobble[16] and the presence of the Stickney crater, an event that would have shattered Phobos completely if it had been a monolith or a complete rubble pile, but would have left a weakly connected Phobos intact[22]. For Phobos, we use Q_2 values based on viscosity estimates and granular friction studies[23] of loose aggregates, whereas k_2 is computed numerically for a two-layer model comprising a consolidated core and a porous outer layer, each of which is half the satellite radius. Since $\mu \gg \rho g R$ (where μ is the shear rigidity modulus, ρ is the mean density and g is the surface gravity) for both satellites, k_2 and Q_2 of Deimos can be approximated by size-scaling it to Phobos[23].

The evolution of planetocentric distances, eccentricities, semi-major axes and inclinations of the two satellites is shown in Fig. 1 for a set of loosely connected aggregate satellite models. Several important observations can be made. First, the evolution of R_p shows that the satellites' orbits intersected, depending on their $K_l^{\prime}$, between 1 Gyr and 2.7 Gyr ago and that this intersection happened close to or above the synchronous radius (Fig. 1a). Second, both satellite orbits were initially eccentric and became gradually circularized by tidal dissipation in Mars and the moons (Fig. 1b). Yet, throughout the integrations, the eccentricities remained small enough (<0.35), reducing the possibility of chaotic tumbling[24,25] or chaotic transitions between spin–orbit resonances[17,24]. Third, Phobos's and Deimos's semi-major axes (Fig. 1c) remained below and above the synchronous radius, respectively. Although counterintuitive, this fact agrees well with our scenario because of the eccentricity values involved. Note that a common origin becomes possible when the maximal value of Phobos's planetocentric distance becomes equal to the minimal value of Deimos's distance. From the planetocentric inequality referred to earlier, we see that, although a must obey $R_p/(1+e) < a$, it nevertheless can stay below R_p. Thus, in the course of our backward integration, Phobos's R_p can become larger than the synchronous radius, with its a value remaining less than this radius. Fourth, the changes in the orbital inclinations are found to be small (<0.021 rad) throughout their entire history (Fig. 1c inset).

Figure 1a shows that the orbits intersected close to or above the synchronous radius (distance range 5.9–6.9 R_{Mars}) from as recently

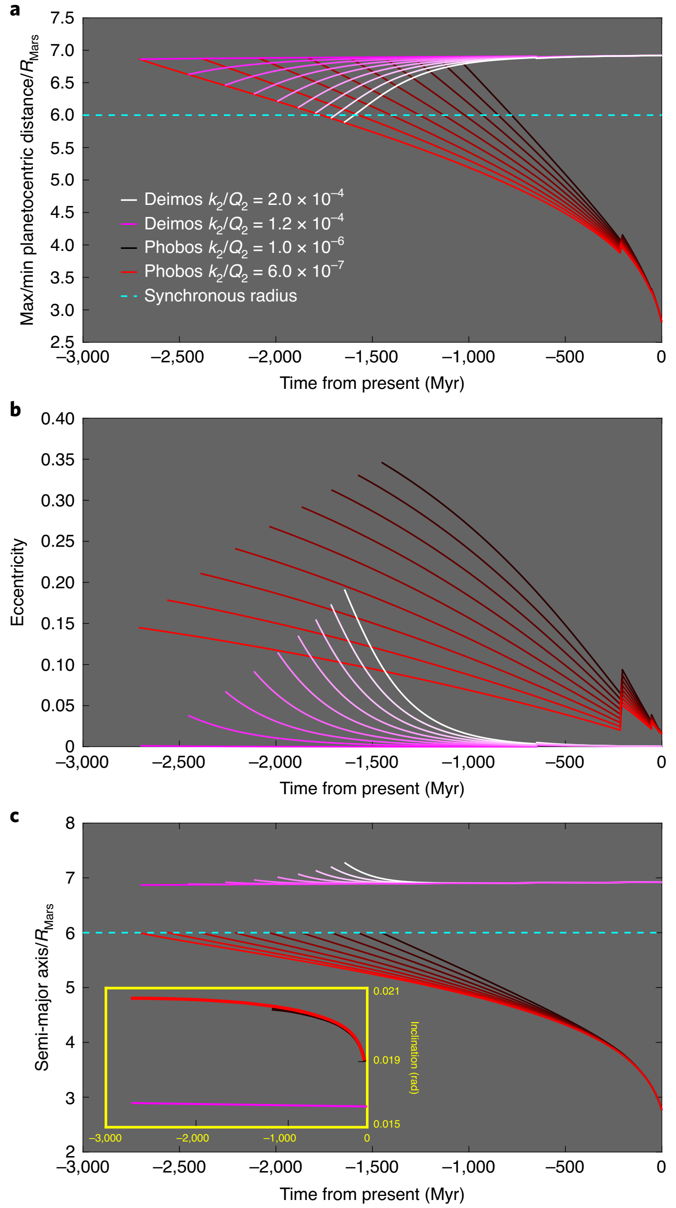

Fig. 1 | The orbital history of Phobos and Deimos. a, Tidal evolution (backward integrated over time) of the planetocentric distance for a set of loosely connected aggregate models of Phobos and Deimos (defined by k_2/Q_2; Supplementary Table 1), with the tidal dissipation inside both Mars and the satellites included; k_2/Q_2 for the individual Phobos and Deimos curves span the end-member range indicated in the legend linearly. **b**,**c**, Corresponding eccentricity (**b**) and semi-major axes (**c**) curves. The eccentricity jumps are due to resonance interactions (see main text) that result in rapid changes in planetocentric distances. Since R_p resides within the interval $a(1-e) \leq R_p \leq a(1+e)$, the curves in **a** for Phobos and Deimos correspond to the maximal and minimal planetocentric distances, respectively. The point where the orbits intersect, that is, where minimal $R_p^{Deimos} \leq$ maximal R_p^{Phobos}, is indicative of a common origin. Both the planetocentric distance and semi-major axis are normalized to R_{Mars}. The inset in **c** shows a plot of the backward-integrated tidal evolution of the inclinations relative to Mars's equator of the moons for the end-member cases (for Deimos, the end-members are superimposed). The smallness of the inclination over the entire lifetime is justified since in the course of uniform equinoctial precession of an oblate host planet, the inclination of a near-equatorial satellite follows the evolving equator, with very small oscillations about it (Supplementary Section 2). Because of the resonances between Phobos and Mars, Phobos and the Sun, and Phobos and Deimos, rapid eccentricity changes have occurred over the past ~650 Myr (**b**).

as 1 Gyr ago, for less consolidated aggregates, to 2.7 Gyr ago, for more consolidated bodies. This suggests a common provenance (in space and time) in the form of a larger progenitor[2,26] that disintegrated to produce Phobos and Deimos. Different initial eccentricities of the satellites (Fig. 1b) support an impact disruption, since post-collisional planetesimal fragments generally vary widely in eccentricity[8]. The subsequent orbital evolution has separated the satellites in space, providing a natural explanation for their current orbital configuration. The low initial orbital inclinations found here favour an equatorially orbiting parent body formed in situ[6–9]. Although the details of the disruption process require more study, it has already been demonstrated that subcatastrophic low-energy disruptive events could result in two main fragments[27]; had more been produced, the remaining debris could have fallen onto Mars[28,29], contributing to what we observe as the Martian cratering record (Supplementary Section 5).

Contrary to popular belief[4,17], the orbits of both bodies may have started above the synchronous radius (Supplementary Section 6 and Supplementary Figs. 2 and 3). The curves show that dissipation inside Phobos is strong enough to drive it through the synchronous limit on its descent towards Mars. This happens when the orbital evolution is dominated by dissipation in the satellite, as the eccentricity stays high enough. In contrast, dissipation inside Deimos is initially only large enough to make it descend within the vicinity of its current orbit. Hence, Deimos's distance to Mars has not been monotonically increasing with time, as is presently the case, but initially evolved inwards. As the eccentricities decreased, so did the dissipation rate in the satellites, and the orbital evolution became governed mainly by dissipation in Mars. Consequently, the inward motion of Deimos changed to outward migration, while dissipation in Phobos was and still is intensive enough that it keeps descending. The case of crossing satellite orbits was considered earlier[5], but was ruled out, partly due to the difficulty of circularizing Deimos's orbit within the lifetime of the Solar System. This difficulty resulted from: the application of a simplistic tidal model (inappropriate for $e > 0.15$) that ignores libration (Supplementary Section 7 and Supplementary Fig. 4) and resonance interactions; the use of ad hoc viscoelastic rheologies based on the limited geophysical data then available; and the application of too small K_l' values.

To test the variation of Phobos's tidal lifetime with initial conditions, we considered low ($e = 0.015$), medium ($e = 0.15$) and high ($e = 0.3$) starting eccentricities, and integrated its orbit forwards in time from the synchronous radius. The results (Supplementary Section 8 and Supplementary Fig. 5) indicate that a satellite with an initial eccentricity <0.2 would crash into Mars in <3.1 Gyr. For any higher initial eccentricity, Phobos's lifetime would be <2 Gyr. A short-lived Phobos presents an obstacle to it having formed alongside Mars. The progenitor, conversely, could have been billions of years old before breaking up, provided that its eccentricity was low, since tidal evolution in the vicinity of the co-rotation radius is slow. Those of its remnants which were born with a sufficient eccentricity (such as Phobos) were dissipative enough to descend and cross the synchronicity radius.

These results provide additional support for the assertion that the satellites cannot be monoliths. Indeed, had the moons been monolithic, the dissipation in them would have not been sufficient to dampen the eccentricity jumps associated with the above-mentioned resonances (Supplementary Section 9 and Supplementary Fig. 6). The backward integration of the orbits indicates that for the eccentricity excursions to become efficiently damped, k_2/Q_2 needs to be at least ~10^{-7} and ~10^{-4} for Phobos and Deimos, respectively, which is achievable only in the case of sufficiently fractured and therefore dissipative moons. Thus, although early accretion[6–9,30] of the Martian moons cannot entirely be ruled out, our results indicate that only in the extreme case of a monolithic Phobos and a very low frequency exponent ($\alpha \approx 0.1$) for dissipation in Mars, which appears to contradict the geophysical observations[11,12,14,21,22], would it be possible to move the origin of Phobos beyond 4 Gyr ago (α is discussed in Supplementary Section 10 and Supplementary Fig. 7).

The effects of past increases in temperature in a previously hotter and therefore more dissipative Mars[30] are shown, for both loose and more consolidated satellites, with both low and high eccentricities in Supplementary Section 11 and Supplementary Figs. 8 and 9. They suggest earlier encounters relative to the nominal case. Any dissipation not accounted for here (for example, a possible early presence of oceans on or melt inside Mars[30], or chaotic tumbling of the satellites[24,25]) would move the origin of the moons closer to the present. Consequently, our results represent lower bounds on their orbital history.

Finally, forward integration to assess the future fate of the satellites (Supplementary Section 12 and Supplementary Fig. 10) shows that, while Deimos very slowly continues to ascend, Phobos will impact on Mars in ~39 Myr (refs. [10,31]) or tidally disintegrate into a ring on reaching the Roche limit. The results presented here stand to be improved with Mars InSight geophysical data, in particular the dissipation in Mars and its frequency dependence that control the orbital history of Phobos. The upcoming Martian Moons Exploration mission will also provide crucial information on the moons' interiors, which will help to settle the question of their origin.

Methods

Orbital evolution theory. The time evolution of each orbital parameter of the two-body system can be cast as

$$\left(\frac{\mathrm{d}x}{\mathrm{d}t}\right) = \left(\frac{\mathrm{d}x}{\mathrm{d}t}\right)^{\text{main}}_{\text{planet}} + \left(\frac{\mathrm{d}x}{\mathrm{d}t}\right)^{\text{main}}_{\text{satellite}} + \left(\frac{\mathrm{d}x}{\mathrm{d}t}\right)^{\text{libration}}_{\text{satellite}}, \tag{4}$$

where x is either a or e. The three terms refer, respectively, to the tides in the planet, the tides in the satellite (with no libration taken into account) and the input from the satellite's libration. In the following, we provide only the main formulae for the orbital evolution. For the full derivations, see Supplementary Section 13. The semi-major axis rate is

$$\begin{aligned}\frac{\mathrm{d}a}{\mathrm{d}t} &= -2an\sum_{l=2}^{\infty}\sum_{m=0}^{l}\frac{(l-m)!}{(l+m)!}(2-\delta_{0m})\sum_{p=0}^{l}\sum_{q=-\infty}^{\infty}\sum_{s=-\infty}^{\infty}\sum_{j=-\infty}^{\infty}\\ &G_{lpq}(e)G_{lpj}(e)(l-2p+q-s)\left[\left(\frac{R}{a}\right)^{2l+1}\frac{M'}{M}F^2_{lmp}(i)K_l(\beta)+\left(\frac{R'}{a}\right)^{2l+1}\right.\\ &\left.\frac{M}{M'}J_{j-q+s}(m\mathcal{A})J_s(m\mathcal{A})F^2_{lmp}(i')K_l(\beta')\right],\end{aligned} \tag{5}$$

where $G(e)$ are the eccentricity functions (Supplementary Table 2), $F(i)$ are the inclination functions, J_s is the order-s Bessel function, β is the tidal mode and all of the other variables are as defined for equations (1)–(3). Since the inclinations of the orbits remain small, only F_{201} and F_{220} are relevant and are equal to 1/2 and 3, respectively. Similarly to $\mathrm{d}a/\mathrm{d}t$, the general expression for the eccentricity rate is

$$\begin{aligned}\frac{\mathrm{d}e}{\mathrm{d}t} &= -\frac{1-e^2}{e}\frac{n}{MM'}\sum_{l=2}^{\infty}\sum_{m=0}^{l}\frac{(l-m)!}{(l+m)!}\\ &\times(2-\delta_{0m})\sum_{p=0}^{l}\sum_{q=-\infty}^{\infty}\sum_{s=-\infty}^{\infty}\sum_{j=-\infty}^{\infty}\\ &G_{lpq}(e)G_{lpj}(e)(l-2p+q-s)\left[\left(\frac{R}{a}\right)^{2l+1}\frac{M'}{M}F^2_{lmp}(i)K_l(\beta)+\left(\frac{R'}{a}\right)^{2l+1}\right.\\ &\left.\frac{M}{M'}J_{j-q+s}(m\mathcal{A})J_s(m\mathcal{A})F^2_{lmp}(i')K_l'(\beta')\right]-\frac{\sqrt{1-e^2}}{e}\frac{n}{MM'}\sum_{l=2}^{\infty}\\ &\sum_{m=0}^{l}\frac{(l-m)!}{(l+m)!}(2-\delta_{0m})\sum_{p=0}^{l}\sum_{q=-\infty}^{\infty}\sum_{s=-\infty}^{\infty}\sum_{j=-\infty}^{\infty}G_{lpq}(e)G_{lpj}(e)(l-2p)\\ &\left[\left(\frac{R}{a}\right)^{2l+1}\frac{M'}{M}F^2_{lmp}(i)K_l(\beta)+\left(\frac{R'}{a}\right)^{2l+1}\frac{M}{M'}J_{j-q+s}(m\mathcal{A})J_s(m\mathcal{A})F^2_{lmp}(i')K_l'(\beta')\right].\end{aligned} \tag{6}$$

Due to very slow convergence of the series and the relatively high eccentricities found in this study, we have to include higher-order terms to ensure precision of our results and stability of integration for high eccentricities.

Contribution from tides. In equation (4), the contribution of tides raised by the satellite in the planet is

$$\left(\frac{\mathrm{d}a}{\mathrm{d}t}\right)^{\mathrm{main}}_{\mathrm{planet}} = n\left(\frac{R^5}{a^4}\right)\left(\frac{M'}{M}\right) \times \mathcal{F}(K_l,\ \dot{\theta},\ n,\ e). \quad (7)$$

The 'main' (unrelated to libration) contribution due to the tides raised by the planet in the satellite looks similar:

$$\left(\frac{\mathrm{d}a}{\mathrm{d}t}\right)^{\mathrm{main}}_{\mathrm{satellite}} = n\left(\frac{R'^5}{a^4}\right)\left(\frac{M}{M'}\right) \times \mathcal{F}(K_l^{'},\ \dot{\theta}',\ n,\ e). \quad (8)$$

Here, $\mathcal{F}$ is a function of the eccentricity, the mean motion, the satellite spin rate ($\dot{\theta}'$) and its tidal response

$$\mathcal{F}(K_l^{'}, \dot{\theta}', n, e) = \sum_{i=0}^{9} e^{2i}\left(\sum_{j=-7}^{-1} K_l^{'}\left(jn - 2\dot{\theta}'\right)\varphi_j^{2i} + \sum_{j=1}^{11} K_l^{'}\left(jn - 2\dot{\theta}'\right)\varphi_j^{2i} + \sum_{j=1}^{9} K_l^{'}(jn)\hat{\varphi}_j^{2i}\right). \quad (9)$$

The coefficients φ_j^{2i} and $\hat{\varphi}_j^{2i}$ of the series are tabulated in Supplementary Tables 3 and 4. Note that in these tables, the terms of the series that are not mentioned are equal to zero. The above equations have been derived for the general case, that is, with neither of the bodies assumed to be synchronous. In the specific situation of a synchronized moon, we have $\dot{\theta}' = n$, and therefore the semi-diurnal term in equation (8) vanishes: $K_l(2n - 2\dot{\theta}') = 0$. In the contribution from the planet, the semi-diurnal term vanishes when the satellite is at the synchronous orbit, that is, when $n = \dot{\theta}'$.

Contribution from libration. The contribution from the longitudinal libration of a synchronized satellite is

$$\left(\frac{\mathrm{d}a}{\mathrm{d}t}\right)^{\mathrm{libration}}_{\mathrm{satellite}} = n\left(\frac{R'^5}{a^4}\right)\left(\frac{M}{M'}\right) \times \mathcal{G}(K_l^{'}, n, e, \mathcal{A}), \quad (10)$$

$\mathcal{G}$ being a function of the eccentricity, the mean motion, the libration amplitude and the tidal response

$$\mathcal{G}(K_l^{'}, n, e, \mathcal{A}) = \sum_{i=0}^{17} e^i \sum_{s=1}^{18-i}\sum_{j=1}^{9} \mathcal{A}K_l^{'}(jn)\gamma_i^{j,s}\ . \quad (11)$$

The coefficients $\gamma_i^{j,s}$ are tabulated in Supplementary Table 5. Similarly, to compute the eccentricity evolution, we write down all the inputs entering equation (6). The input generated by the tides in the planet is

$$\left(\frac{\mathrm{d}e}{\mathrm{d}t}\right)^{\mathrm{main}}_{\mathrm{planet}} = -n\frac{M'}{M}\left(\frac{R}{a}\right)^5 \times \mathcal{L}(K_l, \dot{\theta}, n, e), \quad (12)$$

while the 'main' (unrelated to libration) input from the tides in the satellite is

$$\left(\frac{\mathrm{d}e}{\mathrm{d}t}\right)^{\mathrm{main}}_{\mathrm{satellite}} = -n\frac{M}{M'}\left(\frac{R'}{a}\right)^5 \times \mathcal{L}(K_l^{'}, \dot{\theta}', n, e), \quad (13)$$

where the function $\mathcal{L}$ is defined as

$$\mathcal{L}(K_l, \dot{\theta}, n, e) = \sum_{i=1}^{9} e^{2i-1}\left(\sum_{j=-7}^{-1} K_l\left(jn - 2\dot{\theta}\right)\lambda_j^{2i-1} + \sum_{j=1}^{11} K_l\left(jn - 2\dot{\theta}\right)\lambda_j^{2i-1} + \sum_{j=1}^{9} K_l(jn)\hat{\lambda}_j^{2i-1}\right). \quad (14)$$

The coefficients λ_j^{2i-1} and $\hat{\lambda}_j^{2i-1}$ are tabulated in Supplementary Tables 6 and 7. Note that, similarly to $\mathrm{d}a/\mathrm{d}t$, the expression is general, in that neither of the bodies is a priori assumed to be synchronous. For the synchronized Martian moons, the term associated with the semi-diurnal tide in equation (12) vanishes. The input generated by the satellite's longitudinal libration about the 1:1 spin–orbit resonance is

$$\left(\frac{\mathrm{d}e}{\mathrm{d}t}\right)^{\mathrm{libration}}_{\mathrm{satellite}} = n\frac{M}{M'}\left(\frac{R'}{a}\right)^5 \times \mathcal{H}(K_l^{'}, n, e, \mathcal{A}), \quad (15)$$

where the function $\mathcal{H}$ is given by

$$\mathcal{H}(K_l^{'}, n, e, \mathcal{A}) = \sum_{i=-1}^{16} e^i \sum_{s=1}^{18-i}\sum_{j=1}^{9} \mathcal{A}^s K_l^{'}(jn)\eta_i^{j,s}\ . \quad (16)$$

The coefficients $\eta_i^{j,s}$ are tabulated in Supplementary Table 8.

Owing to the satellites' proximity to Mars, degree-3 terms have also been taken into account. Of these, leading are those with $\{lmpq\} = \{3300\}$ and $\{3110\}$:

$$\left(\frac{\mathrm{d}a}{\mathrm{d}t}\right)_{l=3} = -\frac{3}{4}an\left(\frac{R}{a}\right)^7\frac{M'}{M}\left[5(1-12e^2)K_3(3n-3\dot{\theta}) + (1+4e^2)K_3(n-\dot{\theta})\right] + O(e^4) + O(i^2), \quad (17)$$

where O refers to the order of the truncation error. However, we have explored whole groups of terms, those with $lmpq = 330q$ and $lmpq = 311q$. A direct calculation has shown that in both groups, the important terms are those with $q = -1, 0, 1$:

$$\begin{aligned}\left(\frac{\mathrm{d}e}{\mathrm{d}t}\right)_{l=3} = {} & \frac{M'}{M}\left(\frac{R}{a}\right)^7 n \times \left\{\frac{5}{8}e(1-2e^2)K_3(2n-3\dot{\theta})\right. \\ & + \frac{15}{16}e\left(1 - \frac{49}{4}e^2\right)K_3(3n-3\dot{\theta}) - \frac{125}{8}e\left(1 - \frac{113}{10}e^2\right)K_3(4n-3\dot{\theta}) \\ & - \frac{16{,}129}{256}e^3K_3(5n-3\dot{\theta}) + \frac{3}{8}e\left(1 - \frac{11}{2}e^2\right)K_3(-\dot{\theta}) + \frac{3}{8}e\left(1 + \frac{15}{16}e^2\right)K_3(n-\dot{\theta}) \\ & \left. - \frac{27}{8}e\left(1 + \frac{1}{3}e^2\right)K_3(2n-\dot{\theta})\frac{8{,}427}{256}ne^3K_3(3n-\dot{\theta})\right\} + O(e^5) + O(i^2).\end{aligned} \quad (18)$$

Note that here we do not include terms of higher order in the eccentricities, because the overall effect of degree-3 tides is much less than that of degree-2, so such terms can be neglected.

Inclination. Finally, we compute the rate of the orbit inclination on the Martian equator. Given the smallness of both i and its rate, we here keep only the quadrupole (degree-2) terms[32]

$$\frac{\mathrm{d}i}{\mathrm{d}t} = \frac{M'}{M}\left(\frac{R}{a}\right)^5 n \sin i \times \mathcal{I}(K_l, \dot{\theta}, n, i, e), \quad (19)$$

where

$$\begin{aligned}\mathcal{I} = {} & \left[\frac{243}{64}(1+\rho)e^4K_2(-2n-\dot{\theta}) + \frac{27}{16}e^2\left[1+\rho+\left(\frac{11}{4}+\frac{9}{4}\rho\right)e^2\right]K_2(-n-\dot{\theta})\right. \\ & + \frac{3}{4}\left[1+\rho+\left(\frac{7}{2}+3\rho\right)e^2 + \left(\frac{63}{8}+6\rho\right)e^4\right]K_2(-\dot{\theta}) + \frac{3}{16}e^2\left[1-\rho+\frac{1}{4}(1+\rho)e^2\right] \\ & K_2(n-2\dot{\theta}) + \frac{3}{2}e^2\left[1+\rho+\left(\frac{49}{16}+\frac{41}{16}\rho\right)e^2\right]K_2(n-\dot{\theta}) + \frac{3}{4}\left[1-\rho-\left(\frac{9}{2}-5\rho\right)e^2\right. \\ & \left. + \left(\frac{23}{4}-\frac{63}{8}\rho\right)e^4\right]K_2(2n-2\dot{\theta}) - \frac{3}{4}\left[1+\rho-\left(\frac{9}{2}+5\rho\right)e^2 + \left(\frac{11}{16}+\frac{45}{16}\rho\right)e^4\right] \\ & K_2(2n-\dot{\theta}) + \frac{147}{16}e^2\left[1-\rho-\left(\frac{109}{28}-\frac{123}{28}\rho\right)e^2\right]K_2(3n-2\dot{\theta}) - \frac{147}{16}e^2 \\ & \left[1+\rho-\left(\frac{109}{28}+\frac{123}{28}\rho\right)e^2\right]K_2(3n-\dot{\theta}) + \frac{867}{16}(1-\rho)e^4K_2(4n-2\dot{\theta}) \\ & \left. - \frac{867}{16}(1+\rho)e^4K_2(4n-\dot{\theta})\right] + O(i^3) + O(e^6),\end{aligned} \quad (20)$$

with

$$\rho = \frac{MM'na^2}{(M+M')C\dot{\theta}}, \quad (21)$$

where C is the polar moment of inertia of the planet.

Data availability

The data that support the findings of this study are available from the corresponding author on request.

Code availability

The code for computing the orbital evolution is available on request from the corresponding author.

Received: 28 July 2020; Accepted: 8 January 2021;
Published online: 22 February 2021

References

1. Rosenblatt, P. The origin of the Martian moons revisited. *Astron. Astrophys. Rev.* **19**, 44 (2011).
2. Pajola, M. et al. Phobos as a D-type captured asteroid, spectral modeling from 0.25 to 4.0 μm. *Astron. J.* **777**, 127 (2013).
3. Fraeman, A. et al. Spectral absorptions on Phobos and Deimos in the visible/near infrared wavelengths and their compositional constraints. *Icarus* **229**, 196–205 (2014).

4. Lambeck, K. On the orbital evolution of the Martian satellites. *J. Geophys. Res. Planets* **84**, 5651–5658 (1979).
5. Szeto, A. M. Orbital evolution and origin of the Martian satellites. *Icarus* **55**, 133–168 (1983).
6. Craddock, R. A. Are Phobos and Deimos the result of a giant impact? *Icarus* **211**, 1150–1161 (2011).
7. Citron, R. I., Genda, H. & Ida, S. Formation of Phobos and Deimos via a giant impact. *Icarus* **252**, 334–338 (2015).
8. Canup, R. & Salmon, J. Origin of Phobos and Deimos by the impact of a Vesta-to-Ceres sized body with Mars. *Sci. Adv.* **4**, eaar6887 (2018).
9. Rosenblatt, P. et al. Accretion of Phobos and Deimos in an extended debris disc stirred by transient moons. *Nat. Geosci.* **9**, 581–583 (2016).
10. Efroimsky, M. & Lainey, V. Physics of bodily tides in terrestrial planets and the appropriate scales of dynamical evolution. *J. Geophys. Res. Planets* **112**, E12003 (2007).
11. Lognonné, P. et al. Constraints on the shallow elastic and anelastic structure of Mars from InSight seismic data. *Nat. Geosci.* **13**, 213–220 (2020).
12. Giardini, D. et al. The seismicity of Mars. *Nat. Geosci.* **13**, 205–212 (2020).
13. Jackson, I. & Faul, U. H. Grainsize-sensitive viscoelastic relaxation in olivine: towards a robust laboratory-based model for seismological application. *Phys. Earth Planet. Inter.* **183**, 151–163 (2010).
14. Bagheri, A., Khan, A., Al-Attar, D., Crawford, O. & Giardini, D. Tidal response of Mars constrained from laboratory-based viscoelastic dissipation models and geophysical data. *J. Geophys. Res. Planets* **124**, 2703–2727 (2019).
15. Efroimsky, M. Bodily tides near spin–orbit resonances. *Celest. Mech. Dyn. Astron.* **112**, 283–330 (2012).
16. Rambaux, N., Castillo-Rogez, J., Le Maistre, S. & Rosenblatt, P. Rotational motion of Phobos. *Astron. Astrophys.* **548**, A14 (2012).
17. Yoder, C. F. Tidal rigidity of Phobos. *Icarus* **49**, 327–346 (1982).
18. Khan, A. et al. A geophysical perspective on the bulk composition of Mars. *J. Geophys. Res. Planets* **123**, 575–611 (2018).
19. Pätzold, M. et al. Phobos mass determination from the very close flyby of Mars Express in 2010. *Icarus* **229**, 92–98 (2014).
20. Brasser, R. Efficient tidal dissipation in Deimos. *Icarus* **347**, 113791 (2020).
21. Hurford, T. et al. Tidal disruption of Phobos as the cause of surface fractures. *J. Geophys. Res. Planets* **121**, 1054–1065 (2016).
22. Asphaug, E., Ostro, S. J., Hudson, R., Scheeres, D. J. & Benz, W. Disruption of kilometre-sized asteroids by energetic collisions. *Nature* **393**, 437–440 (1998).
23. Nimmo, F. & Matsuyama, I. Tidal dissipation in rubble-pile asteroids. *Icarus* **321**, 715–721 (2019).
24. Wisdom, J. Rotational dynamics of irregularly shaped natural satellites. *Astron. J.* **94**, 1350–1360 (1987).
25. Quillen, A. C., Lane, M., Nakajima, M. & Wright, E. Excitation of tumbling in Phobos and Deimos. *Icarus* **340**, 113641 (2020).
26. Simioni, E., Pajola, M., Massironi, M. & Cremonese, G. Phobos grooves and impact craters: a stereographic analysis. *Icarus* **256**, 90–100 (2015).
27. Jutzi, M. & Benz, W. Formation of bi-lobed shapes by sub-catastrophic collisions—a late origin of comet 67P's structure. *Astron. Astrophys.* **597**, A62 (2017).
28. Singer, S. F. Origin of the Martian satellites Phobos and Deimos. In *Proc. 1st International Conference on the Exploration of Phobos and Deimos* LPI Contribution No. 1377, 36 (Lunar and Planetary Institute, 2007).
29. Hesselbrock, A. J. & Minton, D. A. An ongoing satellite–ring cycle of Mars and the origins of Phobos and Deimos. *Nat. Geosci.* **10**, 266–269 (2017).
30. Samuel, H., Lognonné, P., Panning, M. & Lainey, V. The rheology and thermal history of Mars revealed by the orbital evolution of Phobos. *Nature* **569**, 523–527 (2019).
31. Black, B. & Mittal, T. The demise of Phobos and development of a Martian ring system. *Nat. Geosci.* **8**, 913–917 (2015).
32. Boué, G. & Efroimsky, M. Tidal evolution of the Keplerian elements. *Celest. Mech. Dyn. Astron.* **131**, 30 (2019).

Acknowledgements
We thank G. Kaplan for comments on an earlier version of this manuscript and M. Jutzi for informed discussion on the topic of impact disruption. This work was supported by a grant from the Swiss National Science Foundation (SNSF project 172508 'Mapping the internal structure of Mars'). This is InSight contribution number 96.

Author contributions
A.B., A.K. and M.E. discussed the original idea; A.B. derived and implemented the orbital evolution model, with input from M.E. and A.K.; M.K. helped with implementation of the numerical time-stepping scheme in the orbital evolution model; A.B. performed the simulations and data analysis and produced the figures; the manuscript was written by A.K., A.B., M.E. and M.K., with input from D.G.

Competing interests
The authors declare no competing interests.

Additional information
Supplementary information The online version contains supplementary material available at https://doi.org/10.1038/s41550-021-01306-2.

Correspondence and requests for materials should be addressed to A.B.

Peer review information *Nature Astronomy* thanks Gwenaël Boué, Hidenori Genda and the other, anonymous, reviewer(s) for their contribution to the peer review of this work.